# Automated L-Band Radar System for Sensing Soil Moisture at High Temporal Resolution

Karthik Nagarajan, *Member, IEEE*, Pang-Wei Liu, *Student Member, IEEE*, Roger DeRoo, *Member, IEEE*, Jasmeet Judge, *Senior Member, IEEE*, Ruzbeh Akbar, *Student Member, IEEE*, Patrick Rush, Steven Feagle, Daniel Preston, and Robert Terwilleger

***Abstract*—The ground-based University of Florida L-band Automated Radar System (UF-LARS) was developed to obtain observations of normalized radar backscatter ($\sigma^0$) at high temporal resolution for soil moisture applications. The system was mounted on a 25 m manlift with capabilities of antenna positioning for multi-angle data acquisition and ranging. The RF subsystem of UF-LARS was based upon the established designs for ground-based scatterometers employing a vector network analyzer with simultaneous acquisition of V- and H-polarized returns. System integration and automated data acquisition were enabled using a software control system. Fifteen-minute observations of $\sigma^0$ collected over a growing season of sweet-corn and bare soil conditions in North Central Florida, were used to study the sensitivity of $\sigma^0$ to growing vegetation and near-surface (0–5 cm) soil moisture ($SM_{0-5}$). On average, $\sigma^0_{VV}$ were observed to be 23% higher than $\sigma^0_{HH}$ during the mid- and late-stages of crop growth due to the vertical structure of stems. The correlation between 3-day observations of $SM_{0-5}$ and $\sigma^0_{VV}$ reduced by 55% compared to those obtained for $\leq$ 30-min observations. These findings suggested that data set at high temporal frequencies can be used to develop more realistic and robust forward backscattering models.**

***Index Terms*—NASA Soil Moisture Active Passive (SMAP), radar, soil moisture (SM).**

## I. Introduction

THE complementary information provided by active and passive microwave signatures can be synergistically used across space and time to obtain optimal near-surface soil moisture (SM) estimates. The upcoming Soil Moisture Active Passive (SMAP) mission [1] will combine active and passive observations to provide an SM product at 9–36 km. Existing ground-based radar systems, such as scatterometers described in [2]–[5], have provided daily observations of backscatter to monitor surface roughness and SM changes. These systems are insufficient for studying the high-temporal variations in SM. Availability of frequent radar observations will provide unprecedented information on the dynamics of near-surface soil moisture following events such as precipitation and irrigation. Accurate estimates of SM can be obtained from backscatter models that are validated using ground-based observations collected at high temporal resolutions. Active observations are also impacted by scattering from rough surfaces and vegetation, whose geometry is typically unknown. Radar observations at different azimuthal angles and over dynamic vegetation at high temporal resolution are essential to developing and validating better backscattering models for agricultural land covers, particularly during the high dynamic conditions.

This letter describes the design of the University of Florida L-band Automated Radar System (UF-LARS) and discusses its utility for soil moisture studies. The UF-LARS is capable of obtaining measurements from up to 25 m above ground as frequently as every 10–15 min, as shown in Fig. 1. Three key design elements of the system include: 1) the antenna and the RF (ARF) subsystem, 2) the electro-mechanical positioning (EMP) system, and 3) the software control and data acquisition (SDA) subsystem. Observations of normalized radar backscatter ($\sigma^0$) were collected over a growing season of sweet-corn and bare soil conditions to understand the active signatures of these two terrains at high temporal frequencies. Such high temporal resolutions will significantly advance the retrieval of SM information from active data. In the next section, we describe three major subsystems of UF-LARS.

## II. System Design of the UF-LARS

### A. Antenna and RF (ARF) Subsystem

The ARF subsystem, shown in Fig. 2, is based upon the established designs for ground-based scatterometers employing a vector network analyzer (NWA). The magnitude and phase measuring capability of the vector NWA enables full-polarimetric measurements with the UF-LARS. The use of the Agilent 8753 series of NWA permits the direct access to the NWA's three receiver channels: R, A, and B. The R channel is used to correct for drifts in the NWA and cabling between the NWA placed on the platform of the lift and the radar electronics package located behind the antenna, as shown in Fig. 1. The A and B channels permit the simultaneous acquisition of V- and H-polarized returns from the target. A multi-throw PIN switch selects the transmit polarization, either V or H, or an internal path to both receive-channels for monitoring gain drifts

Manuscript received November 26, 2012; revised April 2, 2013 and June 5, 2013; accepted June 15, 2013. Date of publication August 2, 2013; date of current version November 25, 2013. This work was supported by the NASA-Terrestrial Hydrology Program (THP)-NNX09AK29G and internal funds from the University of Florida.

K. Nagarajan, P.-W. Liu, J. Judge, P. Rush, S. Feagle, D. Preston, and R. Terwilleger are with the Center for Remote Sensing, Agricultural and Biological Engineering Department, University of Florida, Gainesville, FL 32611-0570 USA (e-mail: bonwei@ufl.edu).

R. DeRoo is with the Department of Atmospheric, Oceanic and Space Sciences, University of Michigan, Ann Arbor, 48109-2143 MI USA.

R. Akbar is with the University of Southern California, Los Angeles, USA.

Color versions of one or more of the figures in this paper are available online at http://ieeexplore.ieee.org.

Digital Object Identifier 10.1109/LGRS.2013.2270453

Fig. 1. UF-LARS mounted on the 25 m Genie platform. (Inset) Trihedral calibration target made of aluminum.

in the amplifier and for internal calibration. The antenna is a custom-designed dual-polarization horn antenna with a custom-designed-turnstile orthmode transducer based upon [6]. These components operate at a center frequency of 1250 MHz, with a bandwidth of 300 MHz and 3 dB beamwidth of 14.7° in the E-plane and 19.7° in the H-plane. The polarization isolation at the center frequency is $>$ 37 dB for all principal planes and decreases to about 23 dB at the band edge of 1400 MHz. The RF electronics and the NWA are maintained at a narrow range of temperature and humidity conditions through actively controlled air conditioning. The 24 cm wavelength of the radar ensures observation of coherent backscattering by the relatively-slow NWA, with a sweep time of 7 min and also even during light wind that causes the vegetation canopy to sway.

### B. Electro-Mechanical Positioning (EMP) Subsystem

The EMP subsystem employs an embedded computer and is composed of three digital inclinometers, an elevation-over-azimuth controller, linear actuators, and a laser range finder, as shown in Fig. 2. One inclinometer is installed on the antenna and two on the X–Y and Y–Z planes of the lift platform. The inclinometers provide incidence angle during scans. The elevation-over-azimuth controller is comprised of an azimuth rotation unit installed on the Genie platform table and the elevation controller mounted on movable brackets attached to the azimuth rotation unit. The system offers a completely automated angular movement of 180° in azimuth and 50° in elevation thereby providing the capability to position the antenna toward any direction for a raster scan. Platform leveling is enabled by controlling three linear actuators installed on the three corners of the platform. A laser range finder, capable of measuring distances up to 50 m at a resolution of 1 mm, is installed on the platform. The system is completely automated enabling continuous data collection, except during external calibration measurements.

### C. Software Control and Data Acquisition (SDA) Subsystem

The SDA subsystem was developed in Visual C++ and is regulated through the state transition diagram that comprised of five distinct states: INITIALIZE, CHECK, RECORD, POSITION, and IDLE. The transitions between the states are enabled by three flags: *Status*, representing the state of platform leveling, *Scans*, the number of cumulative measurements obtained in the current scan, and $t$, representing the elapsed time since last scan. The description of each state and the transitions to subsequent states are shown in Fig. 3. The system was used to obtain measurements over 21 spatial samples in azimuth of an agricultural field every 15 min. Although the measurements were made at a constant incidence angle, the system is capable of continuous elevation scans.

## III. Overview of UF-LARS Signal Processing

Observations of ratios of power received to the power transmitted (power ratios) for the four polarization combinations–VV, HH, HV, and VH polarizations–were recorded as stepped frequency domain measurements. The magnitudes and phases of the raw measurements are altered by both active and passive elements of the ARF subsystem. An internal cal loop was applied to eliminate the gains and losses within the NWA. The fraction of the power ratio that corresponds to backscatter from the target is extracted by time-gating the observations using the range to the target. Measurements of $\sigma^0$ for a target surface was estimated by calibrating the power ratios obtained for the target surface with those from a calibration target with known geometry (see Fig. 1). Observations obtained over a range of azimuth positions and frequency points were averaged to reduce the effects of fading. Each frequency trace is time gated similar to that done on the NWA to minimize the return from the antenna. The trace is multiplied by a Kaiser-Bessel window and inverse Fourier transform is applied. The temporal regions far from the target are zeroed. Fourier transform is applied to the result and is divided by the window to recover the magnitudes of signal in the frequency domain. Even though this reduces the useful bandwidth to 80% of the original bandwidth, undesirable returns, especially from the antenna, are removed. Fig. 4 shows the steps involved in processing the data retrieved from the target. The algorithms used for calibration are described in the following sub-sections.

### A. Internal Radar Calibration (Internal Cal Loop)

The internal calibration was conducted to eliminate the gains and losses from the active and passive components in the NWA. The signal return measurement, $|S_{pt}|^2$, by the NWA is

$$|S_{pt}|^2 = L_{amp} L_{ant} \frac{P_r}{P_t}\bigg|_{pt} \tag{1}$$

where, $L_{amp}$ is the gains and losses of components within NWA, the cabling between NWA and the radar, and the

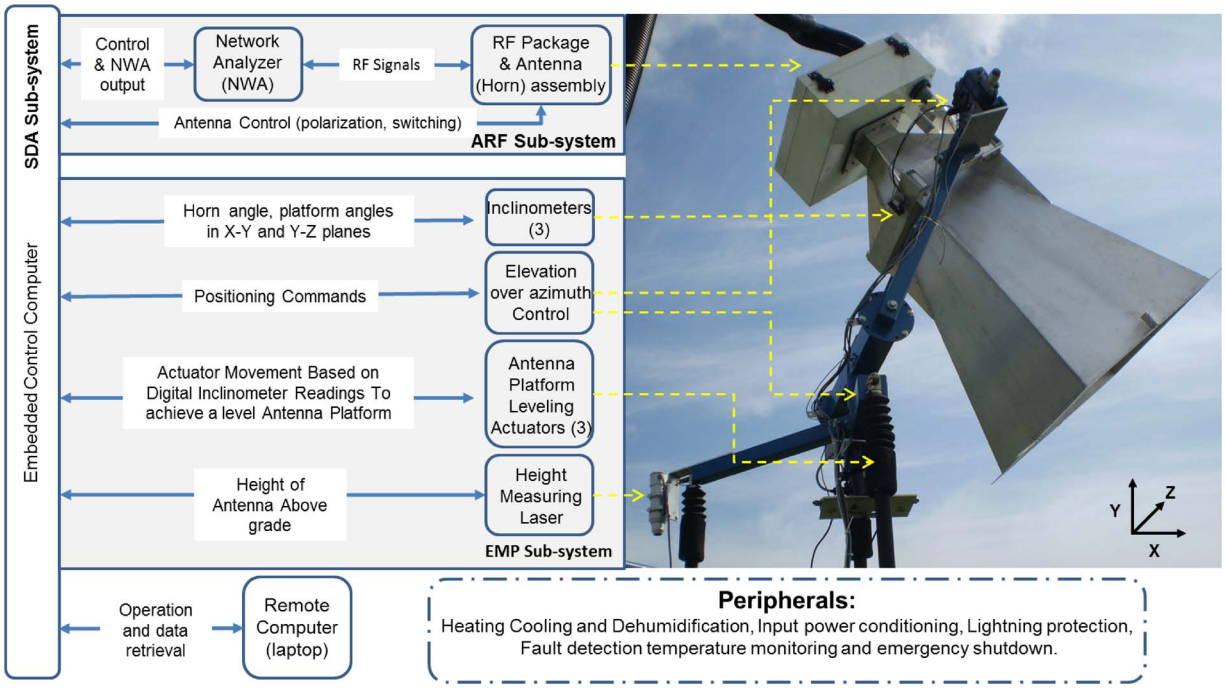


Fig. 2. Subsystems within the UF-LARS.

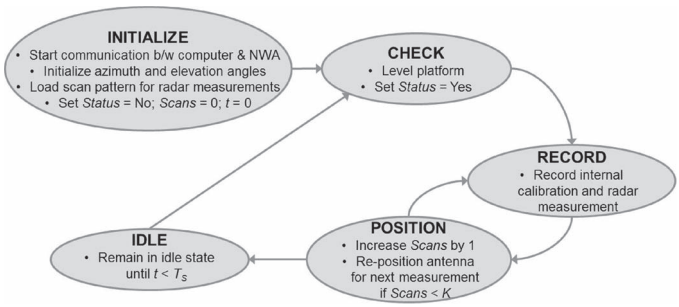


Fig. 3. State transition diagram regulating the SDA subsystem of UF-LARS.

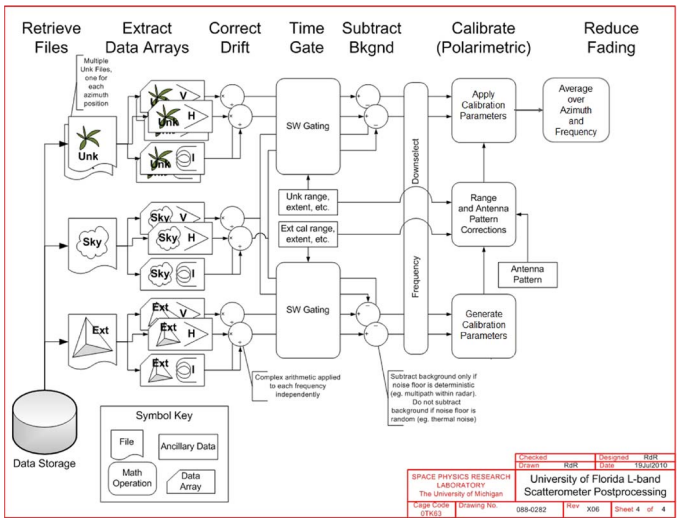


Fig. 4. Postprocessing steps in UF-LARS.

polarization switch, the $L_{ant}$ includes losses from the polarization switch to the aperture and back from the aperture to the internal cal signal coupler, and $P_t$ and $P_r$ are the transmitted and received power of radar. The internal calibration measurement, $|S_{ic}|^2$, coincident with the target measurement is given as

$$|S_{pt}|^2_{ic} = L_{amp} L_{ic} \tag{2}$$

where $L_{amp}$ is same as in (1), and $L_{ic}$ is the losses associated with the internal calibration loop. The signal return measurement is divided by the internal calibration measurement to eliminate the effect by $L_{amp}$ before the further process. $M_{pt}$ represents the power ratio including the gains and losses from $L_{ant}$ and $L_{ic}$, given as

$$M_{pt} = \frac{L_{ant}}{L_{ic}} \frac{P_r}{P_t}\bigg|_{pt}. \tag{3}$$

Because $L_{ant}$ and $L_{ic}$ do not change over time, they will be eliminated by external calibration with a known geometry calibration target.

### B. External Radar Calibration

A trihedral corner–reflector, with an aperture length of 1.28 m, was fabricated for radar calibration (see Fig. 1). It consisted of three triangular aluminum panels, with pores to drain rainwater and minimize wind-effects. The longest side of each triangular panel was reinforced with an angular bar to minimize surface curvature. The point-target radar equation is given in

$$\frac{P_r}{P_t}\bigg|_{cal} = \frac{\lambda^2}{(4\pi)^3} \frac{G_0^2}{R_{cal}^4} \sigma \tag{4}$$

where $(P_r/P_t)\big|_{cal}$ is the power ratio from the calibration target after time gating process, equal to $(L_{ic}/L_{ant})M_{cal}$, $\lambda$ is the wavelength, $\sigma$ is the point-target radar cross section (RCS) obtained using [7], $G_0$ is the maximum antenna gain on boresight, and $R_{cal}$ is the distance from antenna center to the calibration target.

TABLE I
SYSTEM SPECIFICATIONS AT HH, VH, HV, AND VV POLARIZATIONS

| Metric | HH (dB) | VH (dB) | HV (dB) | VV (dB) |
|---|---|---|---|---|
| NE$\sigma^0$ | -23.42 | -48.12 | -38.84 | -25.58 |
| Std. Dev. | 0.17 | 0.56 | 0.34 | 0.14 |
| **Calibration error sources** | | | | |
| | $R_{target}$ | $R_{surface}$ | $\theta$ | $\sigma$ |
| Error in $\sigma^0$ (dB) | $< 0.35$ | $< 0.17$ | $< 0.32$ | $< 1.40$ |

A similar equation for radar return signal from an unknown surface is given in

$$\left.\frac{P_r}{P_t}\right|_{target} = \frac{\lambda^2}{(4\pi)^3} G_0^2 \sigma^0 \int \frac{g^2}{R_{target}^4} dA \tag{5}$$

where $\sigma^0$ is the backscattering coefficient, $(P_r/P_t)\big|_{target}$ is the power ratio from the unknown surface, equal to $(L_{ic}/L_{ant})M_{target}$, $R_{target}$ is the distance to the surface, and $g$ is the antenna gain in the direction of interest, normalized to unity at boresight.

Combining (4) and (5), $\sigma^0$, given in

$$\sigma^0 = \frac{\sigma M_{target}}{M_{cal} R_{cal}^4 \int \frac{g^2}{R_{target}^4} dA} \tag{6}$$

can be calculated using Single Target Calibration Technique (STCT) in [8] for co- and cross-pol.

Equations (4) and (5) were also used to quantify the noise floor, repeatability of the system, and the sources of errors in $\sigma^0$, as shown in Table I. The noise floor was estimated by averaging multiple measurements of $\sigma^0$ obtained while observing the sky. The sky observations indicate the minimum $\sigma^0$ value, Noise Equivalent $\sigma^0$(NE$\sigma^0$), that the UF-LARS is able to measure. Repeatability of the system was measured by the standard deviation of $M_{pt}$ obtained from 69 measurements from 23 targets. Error in the observations of $\sigma^0$ was estimated from independent error contributions from uncertainties in $R_{cal}$, $R_{target}$, $\sigma$, and the incidence angle using the three-standard deviation rule. Uncertainties in $R_{cal}$, $R_{target}$, and the incidence angle were estimated from long term observations of laser range finder and inclinometers. Uncertainty in $\sigma^0$ was estimated using angular errors of inclinometers from geometrical optics model [7]. These uncertainties were integrated into the external calibration (4) and (5), resulting in 2.5 dB error in $\sigma^0$.

## IV. APPLICATION: SOIL MOISTURE SENSING

UF-LARS observed the radar backscatter from growing sweet-corn and an unvegetated agricultural field during the tenth and eleventh Microwave Water and Energy Balance Experiment (MicroWEX-10, -11) in N.C. Florida, from Day of Year (DoY) 186-255, 2011, and DoY 130-160, 2012, respectively. The observations were conducted at an antenna height of 16.2 m above ground and incidence angle of 40°, covering an area equivalent to a 3 dB footprint of $\sim$41 m$^2$, every 15 min. During experiments, soil moisture of 0–5 cm were measured concurrent to the radar observations using Time Domain Reflectometer (TDR) probes, as shown in Figs. 5(a) and 6. These observations were used for analyzing the sensitivity of normalized backscatter to soil moisture. Radar signatures over row-structured agricultural fields are the most sensitive to azimuthal

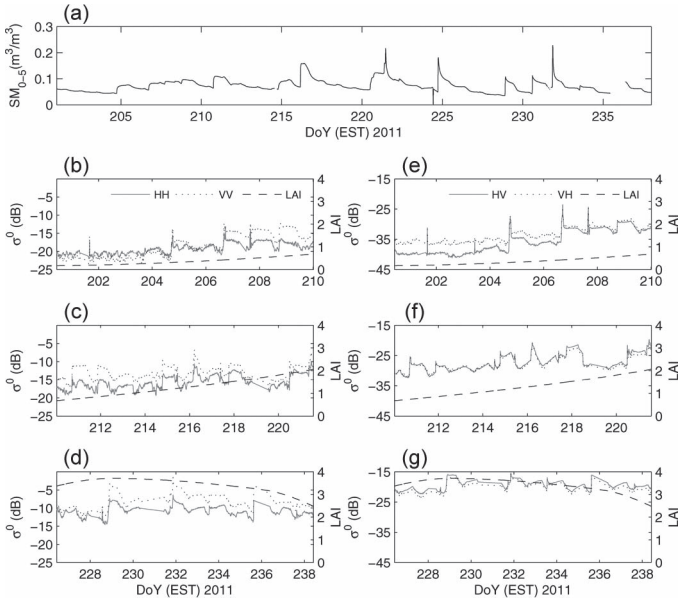


Fig. 5. (a) Observed $SM_{0-5}$, and (b)–(d) $\sigma^0$ at co-pol and (e)–(g) cross-pol during the early (b), (e), mid (c), (f), and late (d), (g) stages of crop growth.

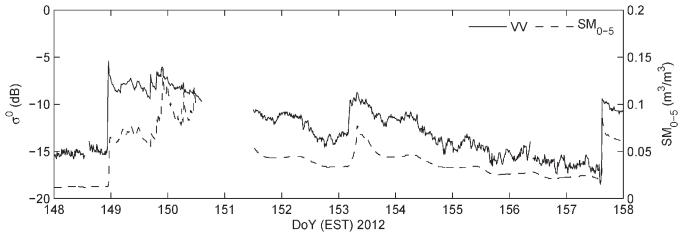


Fig. 6. Variations in $\sigma^0_{VV}$ and $SM_{0-5}$ over bare soil conditions. Precipitation occurred on DoY 149, 150, and 153, and an irrigation occurred on DoY 157.

geometry for angles within 15° of orthogonal to the row direction [9]. Radar signatures are also sensitive to the effects of fading [10] and dynamic land surface conditions such as growing vegetation. To alleviate the above issues, observations of $\sigma^0$ were averaged over five measurements obtained spatially along an azimuthal scan from $-18°$ to 18° at 9° increments, covering about 136 m$^2$, and nine frequency measurements at 30 MHz increments from 1130–1370 MHz at each azimuth angle. The frequency measurements met the spectral independence criteria of $\Delta f \geq (c/2\Delta r)$, where $\Delta f$ is the difference between two adjacent frequencies in Hz, $c$ is the speed of light in m/s, and the $\Delta r$ is the difference between the maximum and minimum ranges from the antenna to the effective illuminated area of the target in meter. In addition, the correlation coefficients among the nine spectral measurements at all four polarization combinations were less than 1/e (0.3679), further confirming their independence. These 45 independent samples reduced the standard deviation of fading from 5.57 to 0.66 dB [11].

### A. Radar Signature Over Growing Vegetation

Observations of $\sigma^0$ obtained at co- and cross-polarizations are sensitive to vegetation cover and to the vertical structure of growing vegetation. The leaf area index (LAI) and $\sigma^0$ observed in co- and cross-polarizations, in Fig. 5, show the similarity in the changes in LAI and $\sigma^0$ over different stages of crop growth. The sensitivity of $\sigma^0$ over growing vegetation can be

TABLE II
MEAN AND SD OF $\sigma^0$ DURING DIFFERENT STAGES OF CORN GROWTH

| Polarization | Metric | Season | | |
|---|---|---|---|---|
| | | Early | Mid | Late |
| HH | Mean | -19.3 | -15.6 | -10.8 |
| | SD | 1.5 | 1.9 | 1.4 |
| VV | Mean | -18.5 | -13.1 | -8.2 |
| | SD | 3.2 | 1.9 | 2.1 |
| HV | Mean | *-35.7 | -27.2 | -19.5 |
| | SD | 3.9 | 2.7 | 1.6 |
| VH | Mean | -33.5 | -27.5 | -20.2 |
| | SD | 2.6 | 2.4 | 1.6 |

*Indicates an observation close to the noise floor for this polarization.

TABLE III
CORRELATION BETWEEN $SM_{0-5}$ AND $\sigma^0_{VV}$ FOR VARYING TEMPORAL RESOLUTION. $\rho$, $\rho_p$, AND $\rho_i$ REPRESENT THE COEFFICIENT DURING THE WHOLE BARE SOIL PERIOD, A PRECIPITATION EVENT, AND AN IRRIGATION EVENT, RESPECTIVELY

| Temporal Resolution | $\rho$ | $\rho_p$ | $\rho_i$ |
|---|---|---|---|
| 15-min | 0.88 | 0.75 | 0.95 |
| 30-min | 0.88 | 0.74 | 0.95 |
| 1-hr | 0.88 | 0.74 | 0.86 |
| 12-hr | 0.72 | - | - |
| 1-day | 0.58 | - | - |
| 2-day | 0.43 | - | - |
| 3-day | 0.40 | - | - |

quantified by analyzing 15-min observations of $\sigma^0$. The mean and standard deviation (SD) of $\sigma^0$ in HH ($\sigma^0_{HH}$), VV ($\sigma^0_{VV}$), HV ($\sigma^0_{HV}$), and VH ($\sigma^0_{VH}$) polarizations for early, mid, and late stages, are given in Table II. During the early stage, $\sigma^0_{HH}$ and $\sigma^0_{VV}$ are similar with mean values of $-19.3$ dB and $-18.5$ dB, respectively. A larger SD is observed in $\sigma^0_{VV}$ compared to $\sigma^0_{HH}$ because of its stronger sensitivity to growing corn than $\sigma^0_{HH}$ toward the end of the early stage (DoY 206-210), as seen in Fig. 5(b). In the mid- and late-stages, the vertical structure of the crop leads to stronger returns in $\sigma^0_{VV}$ than in $\sigma^0_{HH}$ [see Fig. 5(c) and (d)]. A mean difference of 2.5 dB was observed between $\sigma^0_{HH}$ and $\sigma^0_{VV}$, over the mid- and late-stages. The cross-polarization signatures, $\sigma^0_{HV}$ and $\sigma^0_{VH}$, were significantly lower than $\sigma^0_{HH}$ and $\sigma^0_{VV}$ throughout the season as seen in Fig. 5(e)–(g).

### B. Radar Signature Over Dry-Down Periods

The dynamic variations in soil moisture following precipitation and irrigation events and the sensitivity of $\sigma^0$ to these variations were analyzed from the high temporal data obtained from UF-LARS. Fig. 6 shows $\sigma^0_{VV}$ along with soil moisture observations in 0–5 cm ($SM_{0-5}$) collected during bare soil conditions. The significance of high temporal resolution $\sigma^0$ measurements can be quantified by estimating the reduction in correlation ($\rho$) between 15-min observations of $SM_{0-5}$ and interpolated observations of $\sigma^0_{VV}$ at different temporal resolutions. As shown in Table III, a strong correlation of 0.88 is obtained between $SM_{0-5}$ and $\sigma^0_{VV}$ for 15-min, 30-min, and 1-hr observations. The $\rho$ reduces by 34% for daily observations and by 55% for 3-day observations in comparison to $\rho$ obtained from observations at 1 hr or less. The above insight is significant considering that measurements from SMAP will be available at 3-day intervals.

Further analyses for correlation coefficients were conducted during, two highly dynamic hydrological conditions during DoY 153.15–153.35 and DoY 157.55–157.75. The first period involved a less intense, longer precipitation event, while the second period involved an intense, short irrigation event. The correlation coefficients for observations were about 0.75 for the 15-, 30-, and 60-min observations. However, during the irrigation period, the correlations for the 60-min observations reduces by 9% in comparison to those obtained from 15- and 30-min observations. Such results demonstrate the advantages of active observations at higher temporal resolution for algorithm development, particularly under dynamic hydrological conditions.

## V. SUMMARY AND CONCLUSION

An automated L-band radar system was used to measure $\sigma^0$ at high temporal resolutions of 10–15 min. The system capabilities included radar platform leveling, antenna positioning for multi-angle data acquisition, and ranging. Observations from the UF-LARS were used to study the sensitivity of $\sigma^0$ to growing vegetation and to $SM_{0-5}$ at high temporal resolutions. $\sigma^0_{VV}$ was more sensitive to the vertical structure of growing vegetation with a mean difference of 2.5 dB observed between $\sigma^0_{HH}$ and $\sigma^0_{VV}$ in the mid- and late-stages of crop growth. In correlating $\sigma^0_{VV}$ and $SM_{0-5}$, a 55% reduction in $\rho$ was observed when 3-day observations were correlated in comparison to observations made at $\leq$ 30 min. The sensitivity studies presented in this letter showcase the potential impact of high temporal resolution radar data on the development of radiative-transfer models in retrieving accurate soil moisture information from active–passive data.

## REFERENCES

[1] D. Entekhabi, E. Njoku, P. O'Neill, K. Kellogg, W. Crow, W. Edelstein, J. Entin, S. Goodman, T. Jackson, J. Johnson, J. Kimball, J. Piepmeier, R. Koster, N. Martin, K. McDonald, M. Moghaddam, S. Moran, R. Reichle, J. Shi, M. Spencer, S. Thurman, L. Tsang, and J. V. Zyl, "The soil moisture active passive (SMAP) mission," *Proc. IEEE*, vol. 98, no. 5, pp. 704–716, May 2010.

[2] F. Ulaby, T. Haddock, J. East, and M. Whitt, "A millimeter network analyzer based scatterometer," *IEEE Trans. Geosci. Remote Sens.*, vol. 26, no. 1, pp. 75–81, Jan. 1988.

[3] P. O'Neill and N. Chauhan, "Truck mounted radar system, Chapter XII," Agricultural Research Service, USDA, 1992, Tech. Rep. [Online]. Available: http://www.ars.usda.gov/Research/docs.htm?docid=10087

[4] D. Singh, K. Singh, I. Herlin, and S. Sharma, "Ground-based scatterometer measurements of periodic surface roughness and correlation length for remote sensing," *Adv. Space Res.*, vol. 32, no. 11, pp. 2281–2286, Dec. 2003.

[5] C. Notarnicola, A. D. Álessio, F. Posa, D. Casarano, and V. Sabatelli, "Use of a C-band ground-based scatterometer to monitor surface roughness and soil moisture changes," *Subsurf. Sens. Technol. Appl.*, vol. 4, no. 2, pp. 187–206, Apr. 2003.

[6] A. Navarinni and T. Pisanu, "L-band orthomode transducer for the sardinia radio telescope," vol. 7014, no. 70147N. Proc. SPIE, 2008.

[7] A. Doerry, "Reflectors for SAR Performance Testing," Sandia National Laboratories, Tech. Rep., 2008.

[8] K. Sarabandi and F. Ulaby, "A convenient technique for polarimetric calibration of single-antenna radar systems," *IEEE Trans. Geosci. Remote Sens.*, vol. 28, no. 6, pp. 1022–1033, Nov. 1990.

[9] M. Dobson and F. Ulaby, "Active microwave soil moisture research," *IEEE Trans. Geosci. Remote Sens.*, vol. GE-24, no. 1, pp. 23–36, Jan. 1986.

[10] F. Ulaby and M. Dobson, *Handbook of Radar Scattering Statistics for Terrain*. Norwood, MA, USA: Artech House, 1989.

[11] D. Hoekman, "Speckle ensemble statistics of logarithmically scaled data," *IEEE Trans. Geosci. Remote Sens.*, vol. 29, no. 1, pp. 180–182, Jan. 1991.